PROCEEDINGS OF SPIE

SPIEDigitalLibrary.org/conference-proceedings-of-spie

Deep defects in InGaN LEDs: modeling the impact on the electrical characteristics

Roccato, Nicola, Piva, Francesco, De Santi, Carlo, Brescancin, Riccardo, Mukherjee, Kalparupa, et al.

Nicola Roccato, Francesco Piva, Carlo De Santi, Riccardo Brescancin, Kalparupa Mukherjee, Matteo Buffolo, C. Haller, J.-F. Carlin, N. Grandjean, M. Vallone, A. Tibaldi, F. Bertazzi, M. Goano, Giovanni Verzellesi, Gaudenzio Meneghesso, Enrico Zanoni, Matteo Meneghini, "Deep defects in InGaN LEDs: modeling the impact on the electrical characteristics," Proc. SPIE 12001, Gallium Nitride Materials and Devices XVII, 1200105 (5 March 2022); doi: 10.1117/12.2606560

SPIE.

Event: SPIE OPTO, 2022, San Francisco, California, United States

Deep defects in InGaN LEDs: modeling the impact on the electrical characteristics

Nicola Roccato[1], Francesco Piva[1], Carlo De Santi[1], Riccardo Brescancin[1], Kalparupa Mukherjee[1], Matteo Buffolo[1], C. Haller[2], J.-F. Carlin[2], N. Grandjean[2], M. Vallone[3], A. Tibaldi[3], F. Bertazzi[3], M. Goano[3], Giovanni Verzellesi[4], Gaudenzio Meneghesso[1], Enrico Zanoni[1] and Matteo Meneghini[1]

[1]Dipartimento di Ingegneria dell'Informazione, Università di Padova, via Gradenigo 6/B, Padova 35131, Italy

[2] Institute of Physics, School of Basic Sciences, Ecole Polytechnique fédérale de Lausanne (EPFL), CH-1015 Lausanne, Switzerland

[3]Politecnico di Torino, Corso Duca degli Abruzzi, 24, 10129 Torino, ITALY

[4]Dipartimento di Scienze e Metodi dell'Ingegneria and Centro En&tech, Università di Modena e Reggio Emilia, via Amendola 2, Pad. Morselli, 42122 Reggio Emilia, Italy

Abstract

Deep defects have a fundamental role in determining the electro-optical characteristics and in the efficiency of InGaN light-emitting diodes (LEDs). However, modeling their effect on the electrical characteristics of the LED is not straightforward**.**

In this paper we analyze the impact of the defects on the electrical characteristics of LEDs: we analyze three single-quantum-well (SQW) InGaN/GaN LED wafers, which differ in the density of defects. Through steady-state photocapacitance (SSPC) and light-capacitance-voltage measurements, the energy levels of these deep defects and their concentrations have been estimated.

By means of a simulation campaign, we show that these defects have a fundamental impact on the current voltage characteristic of LEDs, especially in the sub turn-on region. The model adopted takes into consideration trap assisted tunneling as the main mechanism responsible for current leakage in forward bias.

For the first time, we use in simulations the defect parameters (concentration, energy) extracted from SSPC. In this way, we can reproduce with great accuracy the current-voltage characteristics of InGaN LEDs in a wide current range (from pA to mA).

In addition, based on SSPC measurements, we demonstrate that the defect density in the active region scales with the QW thickness. This supports the hypothesis that defects are incorporated in In-containing layers, consistently with recent publications.

Gallium Nitride Materials and Devices XVII, edited by Hiroshi Fujioka, Hadis Morkoç, Ulrich T. Schwarz, Proc. of SPIE Vol. 12001, 1200105
 · 0277-786X · doi: 10.1117/12.2606560

Introduction

The presence of defects within and close to the active region of InGaN light-emitting diodes (LEDs) has a fundamental role in the efficiency and electric-optical characteristics of the device. First of all, these defects, often energetically located near midgap, can increase the non-radiative recombination, behaving as Shockley-Read-Hall (SRH) recombination centers [1][2], and leading to a reduction in the device efficiency especially at low driving currents. But this is not the only effect that these defects can have: deep traps located in the depleted region, in fact, can favor trap-assisted tunneling (TAT) of carriers and significantly increase the sub turn-on leakage current [3]–[5]. Modeling this physical mechanism is of primary importance for a better understanding on how these defects influence the LED electrical behavior and where they are located energetically and spatially, with the aim of improving the quality of the device epitaxy. In addition, by observing the sub turn-on voltage electrical characteristics during an ageing experiment, it is possible to identify specific degradation processes (such as defect generation and/or diffusion) [6]–[8].

In this paper, we propose a model based on experimental defect characterization. In a first step, we fabricated and characterized three InGaN LEDs that differ only by the single quantum well (QW) width. Through Steady-State Photocapacitance (SSPC) and light-capacitance-voltage (L-CV) measurements we extracted the defect proprieties like energy levels and densities. Besides, we observed that the defect concentration increases with increasing thickness of the QW. This indicates that defects are preferentially incorporated in indium-containing layers, as confirmed in recent studies [9]–[12].

In a second step, relying on previous studies on the topic [13]–[15], we defined a model that emulate the electrical behavior of the device for over ten orders of magnitude (from pA to mA), using trap assisted tunneling as the main mechanism that causes sub turn-on leakage current. The results demonstrate that the defect characterization data obtained through the experimental characterization (SSPC and LCV) can be effectively used to reproduce with great accuracy the current-voltage characteristics of InGaN LEDs.

Samples

The InGaN/GaN LEDs analyzed have been grown on a sapphire substrate by metalorganic vapor phase epitaxy (Figure 1). The active region of the device consists of an undoped single QW, placed between two 7.5 nm barriers ($N_D = 3 \times 10^{18}\ cm^{-3}$) and two spacers. The three samples have the same structure but differ only by the QW width. Its thickness is equal to 1.3 nm, 1.8 nm and 2.4 nm, respectively, for the wafers named A, B and C. The precursor used for InGaN layer are

triethylgallium (TEGa) and trimethyl-indium (TMIn) with nitrogen as a carrier gas. The 7.5 nm GaN barriers have been grown in similar conditions. After the undoped spacer, a p-doped $Al_{0.06}Ga_{0.94}N$ layer was used as electron blocking layer (EBL) with $N_A = 5 \times 10^{18}$ cm^{-3}, followed by a p-doped 180 nm GaN layer with the same doping concentration. The anode contact is made by platinum, which is placed on a p-doped 20 nm GaN layer with $N_A = 2 \times 10^{19}$ cm^{-3}. The epitaxial structure consists of an 800 nm n-doped GaN buffer with $N_D = 3 \times 10^{18}$ cm^{-3}, followed by a super lattice under layer (SL UL) constituted by 24 layers of $Al_{0.17}In_{0.83}N/GaN$ (2.1 nm/1.7 nm). The first 22 layers have a doping concentration equal to $N_D = 3 \times 10^{18}$ cm^{-3}, while the last two ones are over-doped at 1×10^{20} cm^{-3}. The Under Layer (UL) is functional for the incorporation of the defects coming from the GaN buffer layer [1], in order to guarantee a lower concentration of traps in the active region and therefore a better efficiency of the device [15]-[11]. The LEDs area is 300×300 μm^2.

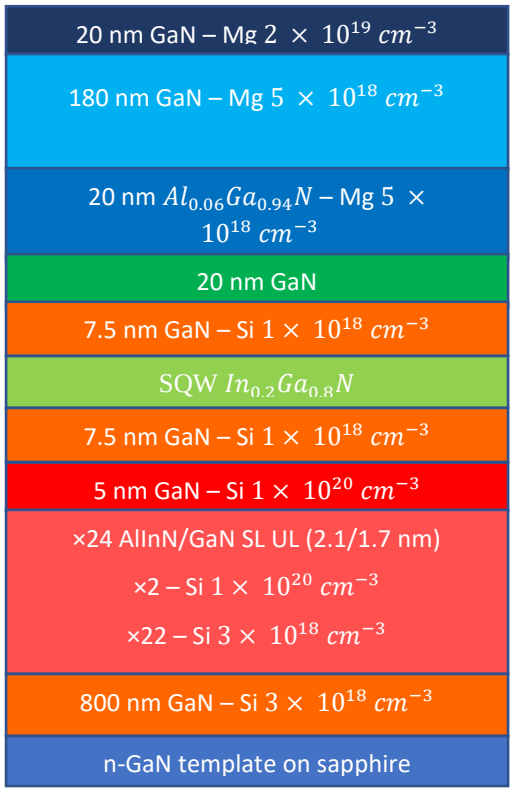

Figure 1: Diagram of the structure of the three LED devices analyzed. They differ only for the thickness of the quantum well, that is: 1.3 *nm*, 1.8 *nm* and 2.4 *nm* respectively for the wafers named A, B and C.

Defect experimental analysis

After a first electrical characterization, carried out by voltage-current measurements (I-V), this experimental analysis concerns the activation energy and density of deep defects respectively through SSPC and LCV measurements.

SSPC determines the energy level of a defect state from the photo-capacitance response due to deep level photoemission. The sample is exposed to sub-band gap monochromatic illumination, generated by a mercury lamp and filtered by a monochromator. An optical fiber and a lens focus the beam forward the sample providing monochromatic excitation in the photon energy range between 1.1 eV and 3.5 eV. A scheme of the adopted setup and of the measurement operation is reported in Figure 2.

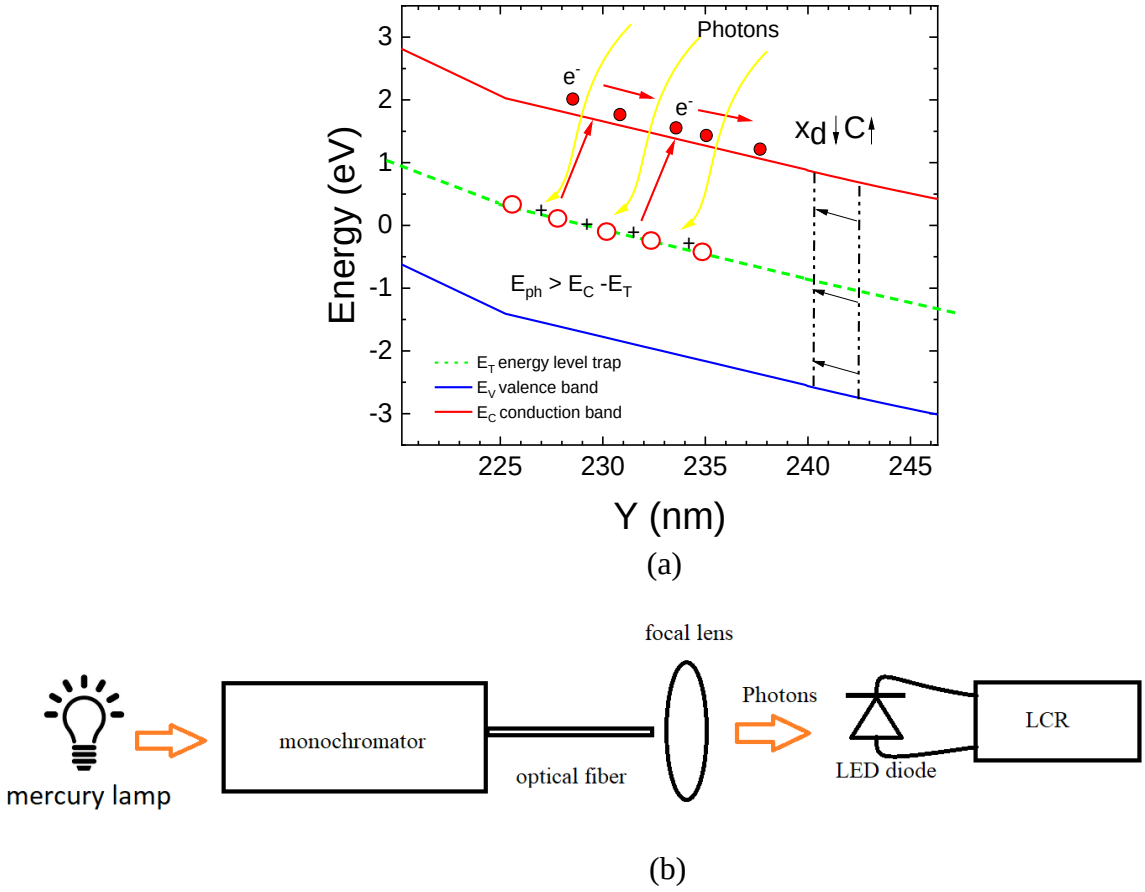

Figure 2: (a) Schematic representation of the procedure used for the steady-state photocapacitance measurements. When monochromatic light hits the sample, electrons are emitted from traps in the space charge region. This results in a reduction in the width of the space charge region, and in the consequent increase in device capacitance. (b) A scheme of the adopted setup.

A photon flux (ϕ) varied between $1-25\times\ 10^{17}\ \mathrm{cm}^{-2}\mathrm{s}^{-1}$ and a bias voltage of 0 V has been adopted in order to grant that the active region is included in the space charge region. In Figure 3 the apparent charge profile as a function of the depletion region is obtained from CV measurements in dark condition. At 0 V the space charge region extends for 46 nm including the QW, the barriers and the spacers. For simplicity in this paper, we defined 'active region' this depletion region, which is the ensemble of the QW and the two surrounding barriers and spacers. The measurements were conducted at room temperature at 1 MHz and the AC-signal amplitude was equal to 50 mV.

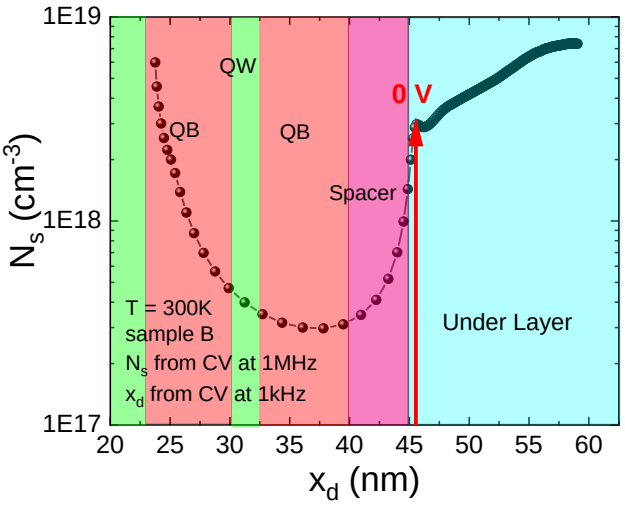

Figure 3: The apparent charge profile as function of depletion region obtained from the capacitance-voltage (CV) measurements in dark condition. At 0 V the depletion region width is *46 nm.*

From the ratio between the time constant obtained from the photo-capacitance transient to the photon flux ϕ, $\frac{1}{\tau\Phi}$, it is possible to extract the deep level photoionization cross-section (PCS) of the traps (see Figure 4). The PCS curves have been fitted by using the model proposed by Passler et al. [16] that allowed us to estimate the optical ionization energy (E^O) and Franck-Condon shift (d_{FC}) of the defect. From these it is possible to obtain the thermal ionization energy E_T calculated as $E_T = E^O - d_{FC}$ as illustrated in Figure 4 (a).

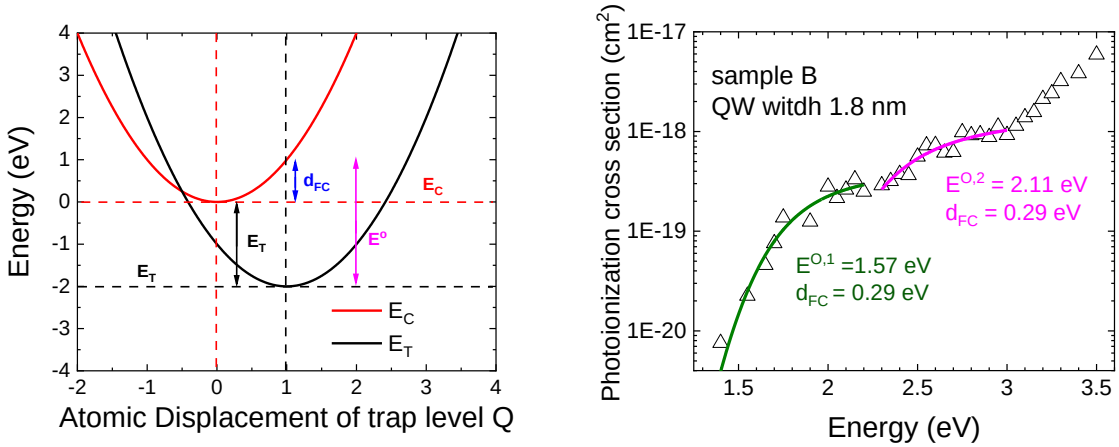

Figure 4: (a) Configuration diagram of the optical and thermal energy level and the Franck-Condon shift energy. (b) Extraction of the defect energy levels using the Passler model on the sample C. Two levels can be clearly identified. The continuous lines represent the fits to Passler model, while the symbols are the photoionization cross section values obtained from the SSPC measurement.

In Figure 4 (b), the PCS of sample B obtained from SSPC measurement is reported, where the solid lines represent the fits according to the Passler model. Two defect levels have been identified, while the change of slope after 3 eV is due to the carrier generation within the QW.

Comparing with the values obtained from the other samples, we observe that the three wafers have the same two deep levels, one with energy in the range 1.28-1.29 eV below the conduction band energy, the other with energy in the range 1.67-1.72 eV below the conduction band energy as we can see in Table 1. It is important to highlight that this measurement does not allow to discriminate in which layer the traps are spatially located, since the width of the depleted region includes both InGaN and GaN layer. For this reason, we consider the possible presence of both the two defects in all layers near the junction. Similar results have been found by Armstrong et al. [17][18][19].

Once identified the same two defects for the three wafers, to quantitatively evaluate the trap densities, Light-Dark CV measurements were carried out. These measurements consist of the repetition of two capacitance-voltage measurements, one performed in dark condition and one under constant monochromatic illumination. The aim is to estimate the additional voltage ΔV required to reach the length of the depletion region x_d when defects are emptied by illumination compared to when the defects are fully occupied. This allow to obtain an estimation of the trap concentration according to the relation [17], [18], [20]:

$$\Delta V = \frac{q}{\epsilon}\int_0^{x_{\{d\}}} x N_T dx$$

Equation 1

and considering N_T constant in the interested region. The measurements were carried out 1 MHz and two different photon energies were used: 1.8 eV and 2.3 eV, in order to extract an estimation of the first defect level and then the second one is obtained as the difference between the concentration estimated at 2.3 eV and the 1.8 eV one.

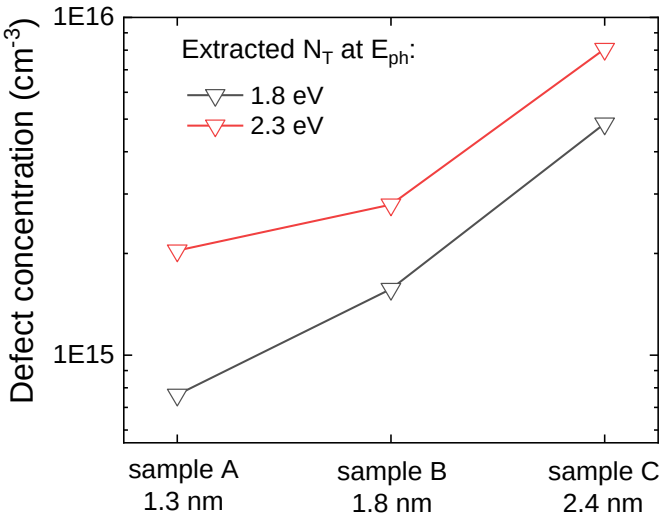

Figure 5: the estimation of the average trap concentration identified at 1.8 eV and 2.3 eV under the conduction band in the active region. It can be notice a rising in the concentration increasing the QW width.

sample	A (1.3 nm)	B (1.8 nm)	C (2.4 nm)
$E_{T,1}$ (eV)	1.29	1.28	1.29
$N_{T,1}$ (cm^{-3})	7.66E14	1.57E15	4.85E15
$E_{T,2}$ (eV)	1.71	1.72	1.67
$N_{T,2}$ (cm^{-3})	1.27E15	1.23E15	3.21E15

Table 1: The thermal activation energy levels for the three analyzed wafers from SSPC measurements, obtained by the difference between the optical activation energy and the Franck-Condon shift and the relative average trap concentration obtained by Light-CV measurements. The concentration at the first level is estimated by setting the photon energy at 1.8 eV, while the concentration of the second level is given by the difference between the estimate obtained at 2.3 eV and the one at 1.8 eV.

In Table 1 and in Figure 5 a summary of the average trap density in the active region (AR), *i.e.* the region including the SQW and the surrounding barriers and spacers is reported. It is worth noticing that, due to the spatial resolution of the measurements, it is impossible to selectively measure just the QW. However, from the data obtained, a monotonic dependence of trap concentration on the QW width can be observed. This increase of defects with the QW thickness is due to the incorporation of defects in In rich layers during the growth, as supported by previous papers [9]–[12], and thus, a wider QW creates a greater amount of defects. In addition to that, the presence of a thicker InGaN QW may impact on the epitaxial strain within the adjacent GaN layers, thus contributing to further increase the defectiveness of the QW but also of the close layers [21]–[24]. Since the defect densities estimated are related to a region (that includes QW+ barriers+ spacers) with the same thickness for all the three wafers, we can conclude that the rise in the defect concentration is related to the increasing of defects incorporated in the QW and close layers due to the increasing on the QW thickness.

Modeling

After this experimental characterization, with the help of Sentaurus TCAD suite from Synopsys Inc., numerical simulations have been performed. The layers of the structure have been doped placing traps (Si and Mg) at their characteristic energy levels, that is, 150 meV from valence band for Mg in GaN (200 meV in AlGaN EBL) and 20 meV from conduction band for Si in GaN [25]–[28]. The main recombination processes have been activated, like Shockley–Read–Hall (SRH), radiative and Auger, and also thermionic emission mechanism has been considered. A parallel resistance ($R_p = 6 \times 10^{10}\ \Omega$) has been added to the device, in order to simulate the current leakage due to parasitic paths, that act in the electrical characteristic at low voltages (near 0 V), while a series resistance ($R_s = 10\ \Omega$) simulates non-idealities due to contacts, buffer layers, partial activation of doping, etc... [29]. Both the values have been extrapolated by the experimental IV characteristics. Finally, the p contact is made of platinum so his work function has been set to 6.35 eV (Φ_M) [30].

The main IV region of interest in this analysis is below the turn-on voltage, which is dominated by leakage current due to the action of trap assisted tunneling process (TAT). This phenomenon is determined by electrons and holes tunneling from respectively the n-type side and the p-type side, towards defect states located mainly within the forbidden bandgap of the undoped spacer. The carriers, reached the traps, recombine non-radiatively, generating the sub turn on leakage current. The traps, thus, act as efficient non-radiative recombination centers. In Figure 6 the simulated band

diagram at equilibrium of the device and a schematic representation of TAT are reported. The experimentally identified defect levels have been placed in the active region (QW, barriers and spacers) and the carriers tunnel from n and p-side respectively for electrons and holes into the recombination centers.

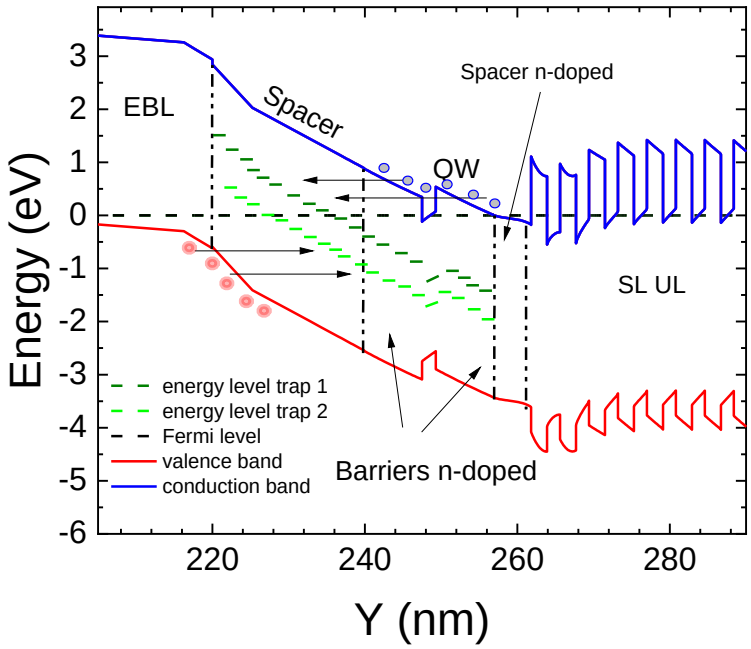

Figure 6: Equilibrium band diagram of the devices analyzed and scheme of the trap assisted tunneling mechanism. The electrons tunnel from n-side forward the traps while holes from the p-side. In the traps, that act as recombination centers, they recombine non-radiatively causing a sub turn-on leakage current.

The model implemented for describing tunneling considers the combination of two capture/emission mechanisms: a phonon-assisted *inelastic* process ($c_{n,p}^{phon}$) and an *elastic* transition ($c_{n,p}^{el}$) [31][15][32][33]. These mechanisms are dependent by the energy level of the traps referred to the intrinsic Fermi level (E_T), the interaction volume of the trap (V_T), the Huang-Rhys factor S, the energy of the phonons involved in the transition ($E_{phon} = \hbar\omega$), the tunneling electron effective mass (m_t) and the number of the phonons emitted in the transition (l). This model for TAT works as an additional SRH recombination rate:

$$R_{TAT} = \frac{N_T c_n c_p (np - n_i^2)}{c_n \left(n + \frac{n_i}{g_n} e^{\frac{E_T}{k_B T}} \right) + c_p \left(p + \frac{n_i}{g_p} e^{\frac{E_T}{k_B T}} \right)}$$

Equation 2

where N_T is the trap density, $g_{n,p}$ are the electron and hole degeneracy factors and $c_{n,p}$ are the capture rates. The values of Huang-Rhys factor S, Huang-Rhys factor S and the energy phonon E_{phon} have been chosen in agreement with the previous papers [15][34][35][36].

Besides, it is worth noting that the superlattice under layer presents AlInN layers. These layers have a wide energy gap equal to 5.17 eV that could obstacle the electron path (Figure 6). This doesn't happen in the real device because these layers are very thin, as confirmed by simulations including barrier tunneling at the heterointerfaces within the UL. This was implemented by using the Wentzel–Kramers–Brillouin (WKB)tunneling probability model, as described in [32].

After setting up the model for trap-assisted tunneling, we evaluated its sensitivity to the main parameters, in order to calibrate it. The traps have been placed with a narrow Gaussian energy distribution, having $\sigma_T = 5$ meV, and the variation of the leakage current has been observed both varying the trap concentration and energy level. With increasing trap density, it can be observed an increasing of the sub turn-on current, according to the Equation 2. While, increasing E_T from the conduction band, a diminution of the onset voltage of the tunneling process can be observed together to a reduction in leakage current near the turn on voltage. This result is due to the variation in the forward voltage that should be applied so that the level of the traps is energetically aligned with the starting interface of the electrons at the conduction band. Thus, a lower voltage may be needed to obtain relatively high tunneling probabilities. Finally, the relative tunneling mass (m_t) and the percentage of piezoelectric activation (PE) of the device has been empirically adapted according with the previous papers [37]–[39]. Once analyzed the sensitivity, the values of the energy levels of the defects and their concentrations have been chosen exactly equal to those obtained from the SSPC and L-CV measurements. In Table 2 the values of the main parameters adopted in the simulations are reported.

Parameter	unit	Sample A	Sample B	Sample C
S		10	10	10
V_T	μm^3	2×10^{-7}	2×10^{-7}	2×10^{-7}

$\sigma_{e,h}$	cm^2	1×10^{-11}	1×10^{-11}	1×10^{-11}
E_{phon}	meV	91.2	91.2	91.2
Φ_M	eV	6.35	6.35	6.35
$E_C - E^T{}_1$	eV	1.29	1.28	1.29
$N_{t,1}$	cm^{-3}	7.66E14	1.57E15	4.85E15
$E_C - E^T{}_2$	eV	1.71	1.72	1.67
$N_{t,2}$	cm^{-3}	1.276E15	1.23E15	3.21E15
$\sigma_{T,1}$	meV	5	5	5
$\sigma_{T,2}$	meV	5	5	5
PE		0.65	0.65	0.65
R_S	Ω	9	10	12
R_P	Ω	6E10	6E10	6E10

Table 2: the main parameters set in the simulations for the three samples.

Results and conclusions

In Figure 7 the simulated IV curves have been reported and compared to measurements. A good agreement with the measured curves has been reached for all the three samples. These results indicate the fundamental importance of defect characterization and of the use of the experimental data in the model in order to reproduce and reach a better understanding of the device behavior. It is worth noting that the deeper level, with activation energy about $E_T = E_C - 1.70$ eV, influences more the IV characteristic because the onset voltage of the tunneling process depend by the near midgap levels, while the other level contributes to slightly increase the leakage current near the turn-on voltage. This is in agreement with previous papers, that suggested that states near midgap, like the detected 1.7 eV level, have a higher TAT probability in LEDs [1][22][5][13].

These results prove that IV characteristics can provide precious information related to the presence of midgap defect placed into the active region, that are also responsible for SRH recombination. Besides, possible variation due to the generation or diffusion of defects during ageing tests could be reproduced and detected with the model. Thus, the combination of a simple log-scaled

experimental I-V plot and a suitable model can be used to get important information on semiconductor quality.

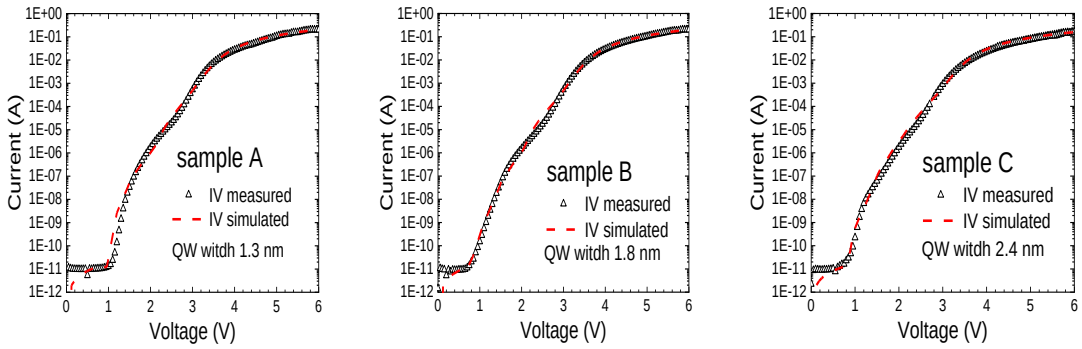

Figure 7: Comparison between the simulated IV curve (red dashed line) and the experimental curve (black symbols) for the three samples. A good reproduction of the real curve has been reached for about ten orders of magnitude, implementing the data obtained by the experimental defects characterization.

To conclude, in this paper we have analyzed three InGaN/GaN LED with super lattice under layer, that differ only by the QW width. After a preliminar electrical characterization, we have performed steady state photocapacitance and light-CV measurements in order to estimate the defect energy levels and concentrations. Two energy levels have been identified for the three sample (at 1.28-1.29 eV and 1.67-1.72 eV from E_C) with a concentration that increases with the QW width, supporting the hypothesis that defects are preferably incorporated in In-rich layers.

With the Sentaurus TCAD simulator a model of the device has been implemented, considering the trap assisted tunneling as the main responsible for sub turn-on leakage current. The same values identified in the experimental characterization have been used into the model and a good correspondence has been reached. This approach could be useful not only for detecting the presence of midgap defects from the model and the IV curves, but also for estimating the defect generation during long-term ageing tests.

Bibliography

[1] G. Verzellesi *et al.*, “Efficiency droop in InGaN/GaN blue light-emitting diodes: Physical mechanisms and remedies,” *Journal of Applied Physics*, vol. 114, no. 7. American Institute of PhysicsAIP, p. 71101, Aug. 21, 2013, doi: 10.1063/1.4816434.

[2] S. F. Chichibu *et al.*, “The origins and properties of intrinsic nonradiative recombination centers in wide bandgap GaN and AlGaN,” *J. Appl. Phys.*, vol. 123, no. 16, p. 161413, Apr. 2018, doi: 10.1063/1.5012994.

[3] N. I. Bochkareva *et al.*, “Defect-related tunneling mechanism of efficiency droop in III-nitride light-emitting diodes,” *Appl. Phys. Lett.*, vol. 96, no. 13, p. 133502, Mar. 2010, doi: 10.1063/1.3367897.

[4] D. P. Han *et al.*, “Nonradiative recombination mechanisms in InGaN/GaN-based light-emitting diodes investigated by temperature-dependent measurements,” *Appl. Phys. Lett.*, vol. 104, no. 15, p. 151108, Apr. 2014, doi: 10.1063/1.4871870.

[5] C. De Santi *et al.*, “Evidence for defect-assisted tunneling and recombination at extremely low current in InGaN/GaN-based LEDs,” *Appl. Phys. Express*, vol. 12, no. 5, p. 052007, May 2019, doi: 10.7567/1882-0786/ab10e3.

[6] X. A. Cao, P. M. Sandvik, S. F. LeBoeuf, and S. D. Arthur, “Defect generation in InGaN/GaN light-emitting diodes under forward and reverse electrical stresses,” *Microelectron. Reliab.*, vol. 43, no. 12, pp. 1987–1991, Dec. 2003, doi: 10.1016/j.microrel.2003.06.001.

[7] J. Liu, H. Wong, S. L. Siu, C. W. Kok, and V. Filip, “Degradation behaviors of GaN light-emitting diodes under high-temperature and high-current stressing,” *Microelectron. Reliab.*, vol. 52, no. 8, pp. 1636–1639, Aug. 2012, doi: 10.1016/j.microrel.2011.09.014.

[8] S. L. Chuang, A. Ishibashi, S. Kijima, N. Nakayama, M. Ukita, and S. Taniguchi, “Kinetic model for degradation of light-emitting diodes,” *IEEE J. Quantum Electron.*, vol. 33, no. 6, pp. 970–979, Jun. 1997, doi: 10.1109/3.585485.

[9] F. Piva *et al.*, “Defect incorporation in In-containing layers and quantum wells: experimental analysis via deep level profiling and optical spectroscopy,” *J. Phys. D. Appl. Phys.*, vol. 54, no. 2, p. 7, Sep. 2020, doi: 10.1088/1361-6463/abb727.

[10] C. Haller, J. F. Carlin, G. Jacopin, D. Martin, R. Butté, and N. Grandjean, “Burying non-radiative defects in InGaN underlayer to increase InGaN/GaN quantum well efficiency,” *Appl. Phys. Lett.*, vol. 111, no. 26, Dec. 2017, doi: 10.1063/1.5007616.

[11] C. Haller *et al.*, “GaN surface as the source of non-radiative defects in InGaN/GaN quantum wells,” *Appl. Phys. Lett.*, vol. 113, no. 11, Sep. 2018, doi: 10.1063/1.5048010.

[12] A. Y. Polyakov *et al.*, “Effects of InAlN underlayer on deep traps detected in near-UV InGaN/GaN single quantum well light-emitting diodes,” *J. Appl. Phys.*, vol. 126, no. 12, 2019, doi: 10.1063/1.5122314.

[13] M. Auf Der Maur, B. Galler, I. Pietzonka, M. Strassburg, H. Lugauer, and A. Di Carlo, “Trap-assisted tunneling in InGaN/GaN single-quantum-well light-emitting diodes,” *Appl. Phys. Lett.*, vol. 105, no. 13, p. 133504, Sep. 2014, doi: 10.1063/1.4896970.

[14] F. Bertazzi *et al.*, “Modeling challenges for high-efficiency visible light-emitting diodes,” in *2015 IEEE 1st International Forum on Research and Technologies for Society and Industry, RTSI 2015 - Proceedings*, Nov. 2015, pp. 157–160, doi: 10.1109/RTSI.2015.7325090.

[15] M. Mandurrino *et al.*, “Physics-based modeling and experimental implications of trap-assisted tunneling in InGaN/GaN light-emitting diodes,” *Phys. status solidi*, vol. 212, no. 5, pp. 947–953, May 2015, doi: 10.1002/pssa.201431743.

[16] R. Pässler, “Photoionization cross-section analysis for a deep trap contributing to current collapse in GaN field-effect transistors,” *J. Appl. Phys.*, vol. 96, no. 1, pp. 715–722, Jul. 2004, doi: 10.1063/1.1753076.

[17] A. Armstrong, T. A. Henry, D. D. Koleske, M. H. Crawford, and S. R. Lee, “Quantitative and depth-resolved deep level defect distributions in InGaN/GaN light emitting diodes,” *Opt. Express*, vol. 20, no. S6, p. A812, Nov. 2012, doi: 10.1364/oe.20.00a812.

[18] A. M. Armstrong, B. N. Bryant, M. H. Crawford, D. D. Koleske, S. R. Lee, and J. J. Wierer, “Defect-reduction mechanism for improving radiative efficiency in InGaN/GaN light-emitting diodes using InGaN underlayers,” *J. Appl. Phys.*, vol. 117, no. 13, p. 134501, Apr. 2015, doi: 10.1063/1.4916727.

[19] A. Armstrong, T. A. Henry, D. D. Koleske, M. H. Crawford, K. R. Westlake, and S. R. Lee, “Dependence of radiative efficiency and deep level defect incorporation on threading dislocation density for InGaN/GaN light emitting diodes,” *Appl. Phys. Lett.*, vol. 101, no. 16, p. 162102, Oct. 2012, doi: 10.1063/1.4759003.

[20] A. M. Armstrong, M. H. Crawford, and D. D. Koleske, “Contribution of deep-level defects to decreasing radiative efficiency of InGaN/GaN quantum wells with increasing emission wavelength,” *Appl. Phys. Express*, vol. 7, no. 3, p. 032101, Mar. 2014, doi: 10.7567/APEX.7.032101.

[21] S. Ploch, T. Wernicke, M. Frentrup, M. Pristovsek, M. Weyers, and M. Kneissl, “Indium incorporation efficiency and critical layer thickness of (2021) InGaN layers on GaN,” *Appl. Phys. Lett.*, vol. 101, no. 20, p. 202102, Nov. 2012, doi: 10.1063/1.4767336.

[22] T. Langer, H. Jönen, A. Kruse, H. Bremers, U. Rossow, and A. Hangleiter, “Strain-induced defects as nonradiative recombination centers in green-emitting GaInN/GaN quantum well structures,” *Appl. Phys. Lett.*, vol. 103, no. 2, p. 022108, Jul. 2013, doi: 10.1063/1.4813446.

[23] H. Wang *et al.*, “Investigation on the strain relaxation of InGaN layer and its effects on the InGaN structural and optical properties,” *Phys. B Condens. Matter*, vol. 405, no. 22, pp. 4668–4672, Nov. 2010, doi: 10.1016/j.physb.2010.08.058.

[24] H. K. Cho, J. Y. Lee, C. S. Kim, and G. M. Yang, “Influence of strain relaxation on structural and optical characteristics of InGaN/GaN multiple quantum wells with high indium composition,” *J.*

Appl. Phys., vol. 91, no. 3, pp. 1166–1170, Feb. 2002, doi: 10.1063/1.1429765.

[25] W. Götz, N. M. Johnson, C. Chen, H. Liu, C. Kuo, and W. Imler, "Activation energies of Si donors in GaN," *Appl. Phys. Lett.*, vol. 68, no. 22, pp. 3144–3146, May 1996, doi: 10.1063/1.115805.

[26] C. Z. Zhao, T. Wei, L. Y. Chen, S. S. Wang, and J. Wang, "The activation energy for Mg acceptor in AlxGa1-xN alloys in the whole composition range," *Superlattices Microstruct.*, vol. 109, pp. 758–762, Sep. 2017, doi: 10.1016/j.spmi.2017.06.006.

[27] Y. Nakano and T. Jimbo, "Electrical Properties of Acceptor Levels in Mg-Doped GaN," *Phys. status solidi*, vol. 0, no. 1, pp. 438–442, Dec. 2003, doi: 10.1002/pssc.200390082.

[28] L. Silvestri, K. Dunn, S. Prawer, and F. Ladouceur, "Hybrid functional study of Si and O donors in wurtzite AlN," *Appl. Phys. Lett.*, vol. 99, no. 12, p. 122109, Sep. 2011, doi: 10.1063/1.3641861.

[29] N. S. Averkiev *et al.*, "Two channels of non-radiative recombination in InGaN/GaN LEDs," *Phys. B Condens. Matter*, vol. 404, no. 23–24, pp. 4896–4898, Dec. 2009, doi: 10.1016/j.physb.2009.08.252.

[30] H. B. Michaelson, "The work function of the elements and its periodicity Related Articles The work function of the elements and its periodicity," *Cit. J. Appl. Phys*, vol. 48, p. 4729, 1977, doi: 10.1063/1.323539.

[31] M. Mandurrino, "Politecnico di Torino Laurea Specialistica in Ingegneria Fisica TCAD Models for Tunneling Processes in Narrow-Gap Semiconductors," 2013.

[32] Synopsys and Inc, "Sentaurus™ Device User Guide," 2015. Accessed: Aug. 02, 2020. [Online]. Available: http://www.synopsys.com/Company/Pages/Trademarks.aspx.

[33] F. Jiménez-Molinos, F. Gámiz, A. Palma, P. Cartujo, and J. A. López-Villanueva, "Direct and trap-assisted elastic tunneling through ultrathin gate oxides," *J. Appl. Phys.*, vol. 91, no. 8, pp. 5116–5124, Apr. 2002, doi: 10.1063/1.1461062.

[34] M. Levinshtein, S. L. Rumyantsev, and M. S. Shur, "Properties of Advanced Semiconductor Materials: GaN, AIN, InN, BN, SiC, SiGe," *Wiley*, 2001. .

[35] A. Alkauskas, M. D. McCluskey, and C. G. Van De Walle, "Tutorial: Defects in semiconductors - Combining experiment and theory," *Journal of Applied Physics*, vol. 119, no. 18. American Institute of Physics Inc., p. 181101, May 14, 2016, doi: 10.1063/1.4948245.

[36] M. Mandurrino *et al.*, "Semiclassical simulation of trap-assisted tunneling in GaN-based light-emitting diodes," *J. Comput. Electron.*, vol. 14, no. 2, pp. 444–455, Jun. 2015, doi: 10.1007/s10825-015-0675-3.

[37] E. J. Miller, E. T. Yu, P. Waltereit, and J. S. Speck, "Analysis of reverse-bias leakage current mechanisms in GaN grown by molecular-beam epitaxy," *Appl. Phys. Lett.*, vol. 84, no. 4, p. 535, Jan. 2004, doi: 10.1063/1.1644029.

[38] M. B. Gonzalez, G. Eneman, G. Wang, B. De Jaeger, E. Simoen, and C. Claeys, "Analysis of the

Temperature Dependence of Trap-Assisted Tunneling in Ge pFET Junctions," *J. Electrochem. Soc.*, vol. 158, no. 10, p. H955, Jul. 2011, doi: 10.1149/1.3614518.

[39] H. Zhang, E. J. Miller, and E. T. Yu, "Analysis of leakage current mechanisms in Schottky contacts to GaN and Al0.25Ga0.75N⁄GaN grown by molecular-beam epitaxy," *J. Appl. Phys.*, vol. 99, no. 2, p. 023703, Jan. 2006, doi: 10.1063/1.2159547.